Soft Matter

Dynamics in Polymers with Phase Separated Dynamic Bonds: The Case of a Peculiar Temperature Dependence

Journal:	*Soft Matter*
Manuscript ID	SM-ART-01-2024-000115.R1
Article Type:	Paper
Date Submitted by the Author:	01-Apr-2024
Complete List of Authors:	Carden, Peyton; The University of Tennessee Knoxville College of Arts and Sciences, Ge, Sirui; University of Illinois Urbana-Champaign Grainger College of Engineering, Materials Science and Engineering Li, Bingrui; Oak Ridge National Laboratory, chemical science division Samanta, Subarna; The University of Tennessee Knoxville College of Arts and Sciences Sokolov, Alexei; University of Tennessee, Department of Chemistry and Physics & Astronomy

ARTICLE

Received 00th January 20xx,

Accepted 00th January 20xx

DOI: 10.1039/x0xx00000x

Dynamics in Polymers with Phase Separated Dynamic Bonds: The Case of a Peculiar Temperature Dependence

Peyton Carden[a], Sirui Ge[b], Bingrui Li[c], Subarna Samanta[a], Alexei P. Sokolov[a,d†]

The topic of polymers with dynamic bonds (stickers) appears as an exciting and promising area of materials science, thanks to their attractive self-healable, recyclable, extremely tough, and super extensible properties. Polymers with phase separated dynamic bonds revealed several unique properties, but mechanisms controlling their viscoelastic properties remain poorly understood. In this work, we present a dynamic analysis of a model polymer system with phase separated hydrogen bonding functionalities. The results confirm that terminal relaxation in these systems is independent of polymer segmental dynamics and is instead controlled by structural relaxations in clusters of stickers. Detailed analysis revealed a surprising result: terminal relaxation time of these systems has weaker temperature dependence than that of structural relaxation in clusters, although the former is slower than the latter. Borrowing the ideas from the field of block copolymers, we ascribed this unusual result to an LCST-like behavior for the miscibility of the stickers in the polymer matrix. The presented results and ideas deepen the understanding of the viscoelasticity for polymers with dynamic bonds, enabling intelligent design of functional materials with desired macroscopic properties.

I. Introduction

Over the past century, polymers have become one of the most widely used materials, thanks to their light weight, ease of large scale processability, and unparalleled tunability of properties. In recent years, polymers functionalized with dynamic bonds have garnered great interest as they offer solutions to many issues associated with traditional polymers, such as the growing need for recyclability and reduced energy for processability [1]. Moreover, the addition of dynamic bonds into polymer systems enables shape memory, super extensibility, extreme toughness, and self-healing capabilities [2-8]. The dynamic bonding functionalities (stickers) include various chemistries ranging from ionic interactions, hydrogen bonding, π-π stacking, metal-ligand, and even dynamic covalent bonds. Among those, polymers with hydrogen bonding functionalities hold a particular value because of an easily tunable interaction strength [9, 10]. In addition, hydrogen bonding functionalities are more stable chemically and are less sensitive to water and unwanted side reactions which may complicate the dynamics and reversibility of other systems [11, 12].

To provide further mechanical reinforcement and decoupling of terminal flow from segmental dynamics, functionalities that phase separate from the polymer backbone can also be incorporated [13-18]. Recent investigations into this sort of system have revealed a mechanism of network rearrangement which can be attributed to structural relaxation in clusters of stickers and to the miscibility difference between the sticker and the polymer matrix [19]. Moreover, it has been revealed that these properties together with the concentration of stickers govern the system dynamics up to the point of single sticker pullout from the cluster, regardless of the polymer molecular weight and architecture [20].

In the present study, we analyse the dynamics and viscoelastic properties of polydimethylsiloxane (PDMS) chains telechelically functionalized with a multi-OH group (Fig 1) which form phase separated sticker clusters. We investigate these systems with a combination of rheology, dielectric spectroscopy, and DSC to probe the dynamic behavior of this system. We utilize X-ray scattering measurements to characterize the arrangement of the clusters within the matrix itself. Our studies revealed that terminal rheological behavior is slower than the structural relaxation in clusters of stickers, but its temperature variations appear slower than that of the relaxation in clusters. These two dynamic processes (terminal relaxation and structural relaxation in clusters) appear to converge upon cooling. We explain this unusual behavior by a peculiar temperature dependence of the Flory-Huggins interaction parameter that is often observed for hydrogen bonding systems. The presented results further expand the horizon for materials design with phase separated dynamic functionalities.

[a] Department of Chemistry, University of Tennessee, Knoxville, Tennessee 37996, United States.
[b] Department of Materials Science and Engineering, University of Tennessee, Knoxville, Tennessee 37996, United States
[c] The Bredesen Center for Interdisciplinary Research and Graduate Education, University of Tennessee, Knoxville, Tennessee 37996, United States.
[d] Chemical Sciences Division, Oak Ridge National Laboratory, Oak Ridge, Tennessee 37830, United States.
† Corresponding author: sokolov@utk.edu
Electronic Supplementary Information (ESI) available: [details of any supplementary information available should be included here]. See DOI: 10.1039/x0xx00000x

II. Experimental

Synthesis of Multi-OH PDMS Polymer

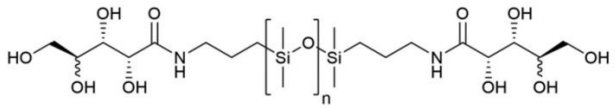

Fig 1. Structure of the studied telechelic multi-OH PDMS chains.

The multi-OH polymers were synthesized using a procedure slightly adapted from Yepremyan et al. [10]. Aminopropyl terminated PDMS with different degrees of polymerization (DP; DP22 sample synthesized with a precursor molecular weight (MW) of ~1600 g/mol, DP50 with MW ~3000 g/mol, and DP74 with MW ~5000 g/mol) was dissolved in 2-propanol and was reacted with D-arabino-1,4-lactone at a 1:2 stoichiometric ratio while stirred at room temperature in a round bottom flask. The 2-propanol was removed using rotovap to leave behind the final viscous samples.

Broadband Dielectric Spectroscopy (BDS)

Dielectric spectra in the frequency range from 10^{-2} to 10^{6} Hz were measured utilizing a Novocontrol Concept-80 system which includes an Alpha-A impedance analyzer and a Quatro Cryosystem temperature control unit. The multi-OH samples were placed into a parallel plate dielectric cell made of sapphire and stainless steel with an electrode diameter of 10 mm, and capacitance ~2.9 pF with an electrode separation of ~220 µm. To prevent crystallization, all samples were quenched from room temperature to about 113 K and reheated to 10 K below the PDMS T_g before the measurements. All the spectra were measured on heating. After each temperature increase, the samples were equilibrated for 10 min to reach thermal stabilization within 0.2 K.

Small Amplitude Oscillatory Shear (SAOS) Rheology

SAOS rheological measurements were utilized to probe the viscoelastic properties of the multi-OH samples through a strain-controlled mode of the AR2000ex (TA Instruments) with an angular frequency range from 10^{2} to 10^{-1} rad/s. We used parallel plate geometry with a disk diameter of 4 mm at a variety of temperatures ranging from T_g of PDMS to temperatures where the sample can flow freely. The strain amplitude during the measurement was chosen to be in the range from 0.03% to 5% depending on the modulus level at different temperatures.

Small Angle X-Ray Scattering (SAXS)

DP22, DP50, and DP70 samples were measured on XEUSS 3.0 (Xenocs, France) equipped with a Cu Kα microfocus source and a Pilatus 300k detector (Dectris, Switzerland). The scattering wavevector (q) was calibrated by a silver behenate standard material. The distance between sample and detector was 0.9 m and 0.55 m for SAXS and WAXS, respectively. The samples were forced into quartz capillaries with a diameter of 1.5 mm and a 0.01 mm wall thickness. These capillaries, as well as an empty reference capillary were placed perpendicular to the X-ray beam. These measurements were taken at room temperature, and the intensity of the empty reference capillary was subtracted from each sample. The noise at intermediate q-range (~0.3-0.5 $Å^{-1}$) appears due to bad statistics at the edge of the SAXS data.

For temperature varied experiments, a reactivity stage was utilized. The samples were allowed five minutes to equilibrate at the desired temperature before the start of the measurements.

Differential Scanning Calorimetry (DSC)

DSC measurements were performed using a Q2500 DSC from TA Instruments. The samples were first equilibrated isothermally at 373 K for 10 min in hermetically sealed pans to remove the thermal history and then cooled to 183 K at a rate of 10 K/min. After equilibration for 10 min, the samples were heated up to 373 K at a rate of 10 K/min. This procedure was repeated twice for each sample to ensure reproducibility.

III. Results

The presence of phase separated clusters in each sample was confirmed using both SAXS measurements (the presence of a peak at the wave vector q ~0.1 $Å^{-1}$, Fig. 2a), and DSC (a calorimetric glass transition (Fig. 3) at temperatures higher than the backbone T_g ~ 145-152K). The SAXS contrast between polymer matrix and functional groups most probably is related to the presence of Si atoms in the polymer backbone. The SAXS peak suggests a well-defined distance between these clusters, however, a relatively large width of this peak suggests no good lattice-like structure. The peak in SAXS spectra shifts to lower q with an increase in DP (Fig. 2a), reflecting, as expected, an increase of the distance between clusters with the increase of the chain length. The peaks at higher q correspond to intersegmental correlations (q~0.85 $Å^{-1}$) and intra-segmental correlations (q~1.5 $Å^{-1}$) of the PDMS backbone [21]. Analysis of the SAXS data does not reveal any particular temperature variations suggesting that the clusters remain intact in the studied temperature range (Fig. 2b). Apparently strong difference in polarity of the end groups and the backbone leads to a stable phase separation in this temperature range (see more details in the Discussion section). Analysis of the peak position near 0.1 $Å^{-1}$ allows estimates of the distance between clusters ($d \approx 2\pi/q_C$). Using these values and assuming that all functional groups are segregated into clusters with a cubic arrangement of clusters, an estimate of cluster radius can be made using equation 1 [22]:

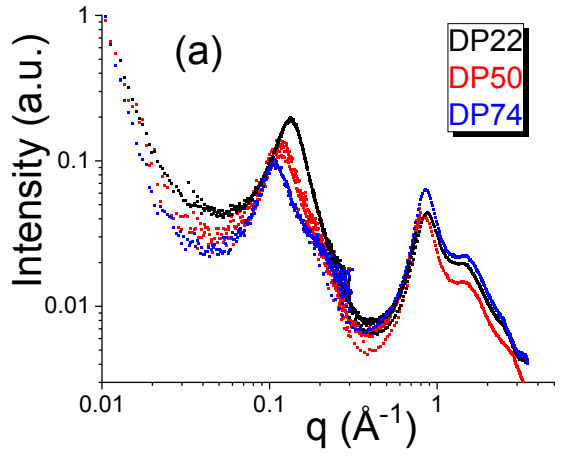

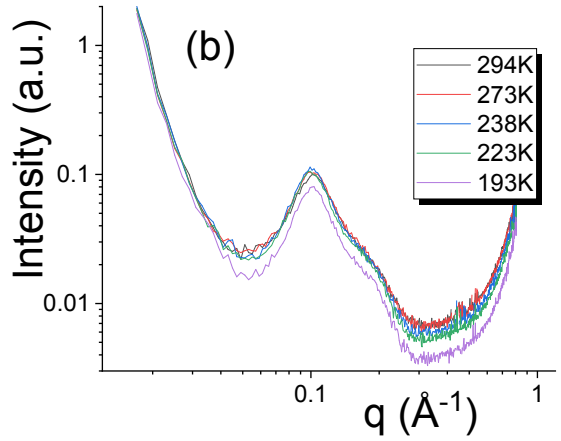

Fig 2: **(a)** X-Ray scattering data for the studied samples at room temperature. The peak at q ~ 0.1 Å^{-1} confirms the presence of phase separated clusters. **(b)** SAXS data for the DP50 sample at various temperatures.

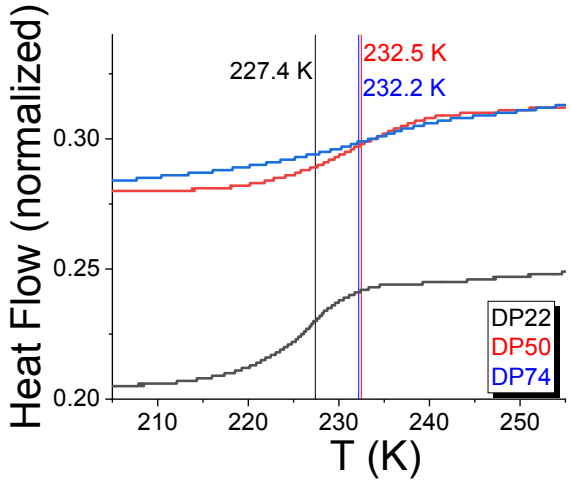

Fig 3. DSC data shows the glass transition at temperatures much higher than the backbone T_g. T_g marked by vertical lines are estimated as the temperature at the middle of the step in the heat flow.

$$R_{cluster} = \frac{d}{2}\left(\frac{6}{\pi} f_e\right)^{\frac{1}{3}} \quad (1)$$

here f_e is the volume fraction of the end groups that we assumed to be equal to the weight fraction. Assuming density in the clusters ~ 1g/cm^3 provides estimates of the number of end groups N_{end} per cluster (Table 1).

The DSC data show a slight change in the cluster T_g and a broadening of the transition with an increase in DP (Fig. 3). The latter might be related to smaller volume fraction of chain ends in samples with larger DP forming smaller size of clusters (see, Table 1).

Table 1. Weight fraction of the end groups, f_e, centre-to-centre distances d and radius $R_{cluster}$ of phase separated clusters, numbers of end groups per cluster N_{end}, T_g of the backbone and of the clusters.

	DP22	DP50	DP74
f_e (wt%)	19	11.2	7.1
d (nm)	4.7	5.3	5.8
$R_{cluster}$ (nm)	1.86	1.71	1.56
N_{end}	85	66	50
Backbone T_g (K), BDS	151.3±0.5	147.7±0.5	146.5±0.5
Cluster T_g (K), BDS		232.2±1	225.1±1
Cluster T_g (K), DSC	227.4±2	232.5±3	232.2±5

Dielectric measurements (Fig. 4) revealed three dynamic processes that we assigned following our earlier studies of similar systems [9, 14, 19, 20]: (1) segmental relaxation (the α-process) caused by change of the monomers dipole orientations during motions of PDMS segments; (2) a dimeric sticker dissociation (α^* process) caused by change of the dipole moment during dissociation of stickers; and (3) a cluster relaxation (α_2 process) caused by change of the dipole moments due to motion of end groups in the clusters. These were present in each sample except the DP22 sample where the α_2-process is hidden by conductivity. Apparently, higher concentration of OH and NH groups in DP22 sample leads to higher conductivity (tail at low frequency in the Fig. 4b). This strong conductivity tail covers the expected at lower frequency α_2-process in BDS spectra of DP22 sample. The peaks in dielectric loss spectra were fit using a Havriliak-Negami function:

$$\varepsilon''(f) = \frac{\Delta\varepsilon}{\left(1 + (i2\pi f\tau_{HN})^a\right)^\gamma} \quad (2)$$

here Δε is the dielectric amplitude of a given process, τ_{HN} corresponds to the characteristic Havriliak-Negami relaxation time of the process, while α and γ represent shape parameters for the given process. The loss peak maximum is traditionally used to estimate the characteristic relaxation time of a relaxation process, and it can be related to the τ_{HN} [23]:

$$\tau_{max} = \tau_{HN}\left(\frac{\sin\left(\frac{\pi\alpha\gamma}{2+2\gamma}\right)}{\sin\left(\frac{\pi\alpha}{2+2\gamma}\right)}\right)^{\frac{1}{\gamma}} \quad (3)$$

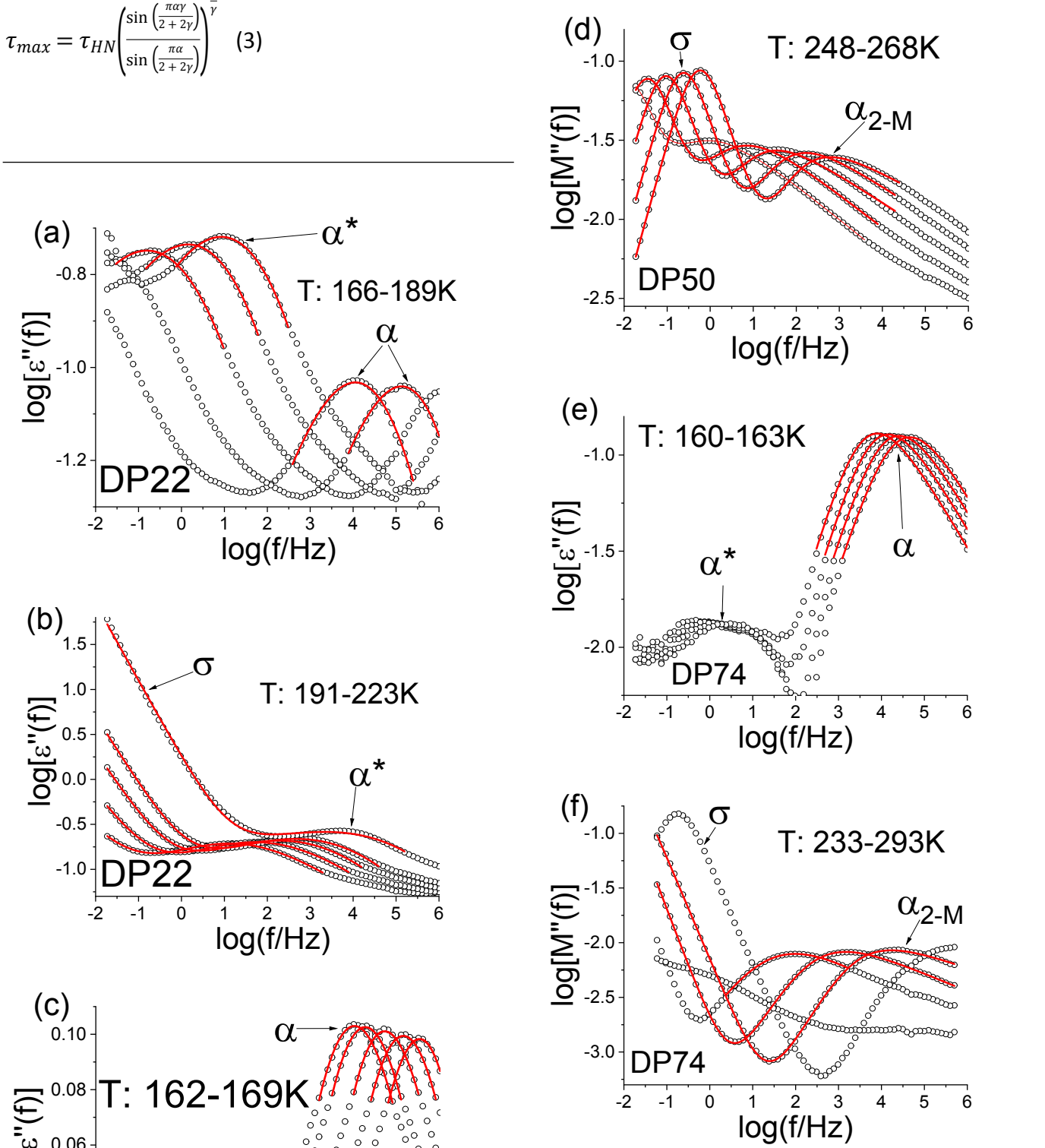

Fig 4. Broadband dielectric spectra (symbols) measured at different temperatures for samples with DP22 **(a, b)**, DP50 **(c, d)** and DP74 **(e, f)**. Lines show fits of the peaks. **(a, c and e)** present the permittivity loss data with α and α* processes, while **(d and f)** present dielectric loss modulus for α* and α_2 processes. The tail of conductivity contribution at lower frequencies covers the α_2 process in spectra of the DP22 sample **(b)**.

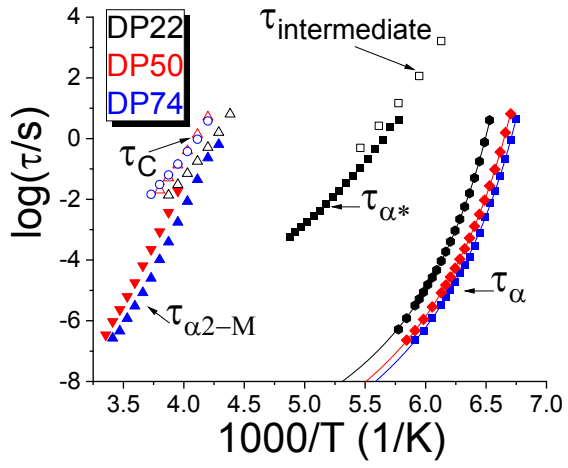

Fig 5. Temperature dependence of characteristic dielectric relaxation times for the segmental (α) process, dimeric sticker dissociation (α*) process, and cluster ($\alpha_{2\text{-}M}$) relaxation (closed symbols) and the rheological intermediate and terminal relaxation times (open symbols). Lines show VFT fits for τ_α(T).

The fastest dielectric process (α-process, Fig. 4) presents PDMS segmental relaxation [9], and extrapolation of its relaxation times to τ_α = 100s provides estimates of the polymer matrix T_g (Table 1). By extrapolating the cluster relaxation times to $\tau_{\alpha 2} = 100\ s$, we can estimate the T_g of the clusters from BDS data. It agrees well with the calorimetric glass transition temperature (Table 1) supporting our assignment of this dielectric process. The α^* process appears strong enough for an accurate fit only in the DP22 sample (Fig. 4). To compare directly BDS and rheological relaxation times, they should be estimated in the same way using, e.g., modulus spectra. To achieve this, the dielectric loss modulus data (Figs. 4d, 4f) instead of the dielectric permittivity[24] are used to estimate the characteristic relaxation time of the α_2 and α^* processes:

$$M^*(\omega) = \frac{1}{\varepsilon^*(\omega)} = M'(\omega) + iM''(\omega) \quad (4)$$

The characteristic times of all the dielectric processes are shown by closed symbols in Figure 5.

Rheology data revealed an extended rubbery plateau in each sample. Its level increases with the decrease of DP as the density of stickers increases (Fig. 6). Master curves of G*(ω) are produced using time-temperature superposition. The time-temperature superposition actually fails in these systems due to different temperature dependence of relaxation processes (Fig. 5). It means that the difference in relaxation times observed in the master curves (Fig. 6) might be misleading. Yet, the obtained master curves serve as a useful qualitative picture presenting different relaxation processes and viscoelastic regimes of the studied systems. The terminal relaxation times are determined as the inverse frequency at which G'(ω) and G"(ω) are crossing. The loss moduli spectra also show an intermediate process (Fig. 6) that was fit using an HN function to determine its relaxation times (Eqs. 2 and 3). To avoid the problems of time-temperature superposition, we estimated characteristic rheological relaxation times only at temperatures when the processes are in the measured frequency range (Fig. 5). The intermediate rheological process has a characteristic time scale comparable to the dimeric dissociation time τ_{α^*}(T) estimated from the BDS data (Fig. 5).

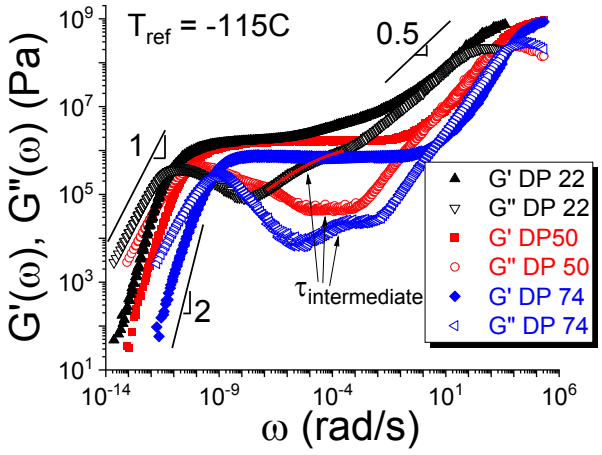

Fig 6. Rheological master curves for each studied sample. The slope 0.5 indicates the Rouse regime at frequencies above the rubbery plateau. The slopes 2 for G'(ω) and 1 for G"(ω) indicate terminal regime. The arrows show intermediate relaxation process in the loss modulus spectra. The line shows an example of the fit of the intermediate relaxation process.

IV. Discussion

We start the discussion with an analysis of the polymer matrix α-relaxation. As has been demonstrated in many publications [20, 25], an increase in sticker concentration leads to a slowing down of segmental relaxation and an increase in the polymer matrix T_g (Fig. 5, Table 1). The latter appears to vary nearly linear with sticker concentration (1/DP), and falls well within the linear dependence seen for other PDMS-based systems regardless of the placement of the stickers on the chain and type of stickers for PDMS [20] (Fig. 7). These results agree well with the recent theoretical predictions for associating polymers with relatively strong sticker associations [25]. The appearance of the binary stickers' dissociation process in the dielectric relaxation data allows estimates of the energy barrier for their dissociation E_a [26-28]:

$$E_a \approx \mathrm{RT} * \ln\left(\frac{\tau_{a*}(T)}{\tau_a(T)}\right) \qquad (5)$$

Here R is the gas constant. The temperature range where experimental data can be measured for both $\tau_\alpha(T)$ and $\tau_{\alpha*}(T)$ is very narrow (Fig. 5), and we extrapolated the data for the $\tau_\alpha(T)$ using Vogel-Fulcher-Tammann (VFT) fit:

$$\tau_\alpha(T) = \tau_0 exp\left(\frac{D}{T - T_0}\right) \qquad (6)$$

with τ_0 fixed to 10^{-12} s. The estimated activation energy for dissociation appears to be ~23 kJ/mol (Fig. 8), which corresponds to breaking ~3-4 hydrogen bonds. Apparently, not all OH and NH groups of the stickers form hydrogen bonding in these binary interactions.

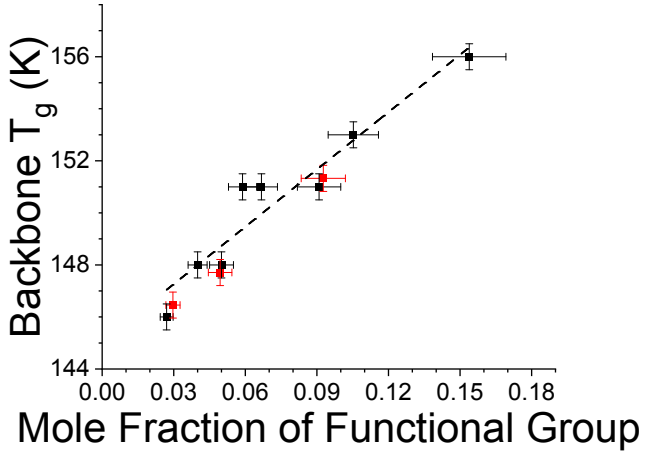

Fig 7. The polymer glass transition temperature vs mole fraction of the functional groups. The red symbols present the system investigated in this work, while the black symbols are from the previous publication [20].

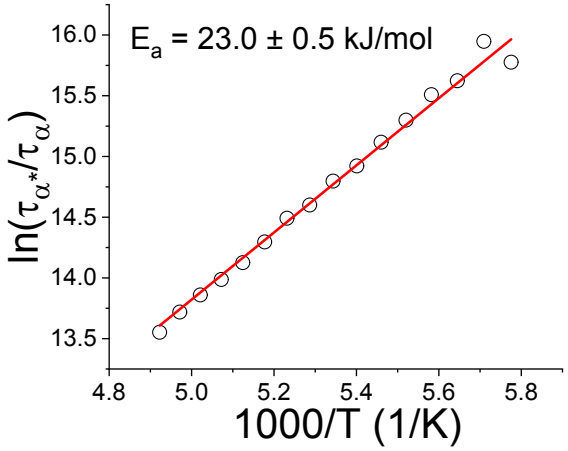

Fig 8. The ratio of relaxation times for the intermediate (dimeric) process, $\tau_{\alpha*}$, and the segmental relaxation time, τ_α, from BDS vs inverse temperature for DP 22 sample. The data for $\tau_\alpha(T)$ were extrapolated to higher temperatures using a VFT fit. The slope provides an estimate of the dissociation energy for the binary interactions of the stickers.

The rheological intermediate process has a characteristic time scale similar to $\tau_{\alpha*}(T)$ from BDS (Fig. 5). The result suggests that this rheological process should be also related to the binary interactions of stickers. It is known, however, that BDS measures the bond dissociation process (change of dipole moment upon bond dissociation) while rheology measures bond rearrangement time [9, 26]. According to the bond lifetime renormalization model [29], these times might differ significantly but will be similar in the case of a strong interaction regime when $E_a >> 2RT*Ln(N)$, here N is the number of backbone segments. Indeed the estimated energy barrier for dissociation appears much higher than 2RT*Ln(N) ~ 6.4 kJ/mol for the DP22 sample [9, 29], and this explains why the bond dissociation time measured by BDS and the bond rearrangement time measured by rheology are very similar (Fig. 5). Unfortunately, α*-process in BDS spectra of DP50 and DP74 samples is weak for detailed quantitative analysis (Figs. 4c, 4e). But its separation from the α-process is similar to that observed in the DP22 sample, suggesting (as expected) the same energy barrier for the binary bond dissociation independent on the backbone molecular weight. In this case, all the samples remain in the strong dissociation energy regime with E_a much larger than 2RT*Ln(N) ~ 9.2 kJ/mol for DP50 and ~10.5 for DP74 samples.

SAXS and rheological data suggest that the majority of stickers are phase separated in clusters, and structural relaxation in these clusters controls the terminal relaxation (Fig. 5). Molecular weight of all studied here systems is significantly below the entanglement molecular weight of PDMS (M_e ~ 15000, i.e. DP ~ 200). Yet, all 3 samples show very extended rubbery plateau with the modulus in MPa range (Fig. 6). This level is significantly higher than in entangled PDMS and is even higher than expected from the molecular weights of PDMS backbone. As has been seen in other phase separated systems, the presence of glassy clusters reinforces the plateau modulus in a mechanism similar to the reinforcement in polymer nanocomposites [13-15]. This additional reinforcement comes from a polymer interfacial layer surrounding glassy clusters that has significantly higher elastic modulus than the pure polymer matrix. It can be well described using the interfacial layer model [13-15], which is out of scope of the current studies. The clusters of stickers work as crosslinks and provide a substantial extension of the rubbery plateau in frequency [13]. It has been suggested in [19] that a single sticker pullout from a cluster controls the terminal relaxation time in telechelic systems. This sticker pullout process is controlled by the structural relaxation in clusters, $\tau_{\alpha 2\text{-}M}$, and an additional energy barrier E_C defined by the miscibility of the polymer matrix and sticker [30-33]:

$$\tau_C(T) = \tau_{\alpha_2-M}(T)\exp\left(\frac{E_C}{RT}\right) = \tau_{a_2-M}(T)\exp\left(\alpha\chi N_s\right) \quad (7)$$

Here χ is the Flory-Huggins interaction parameter between the sticker and the polymer matrix, and N_s is the number of segments in the sticker which we assume to be N_s = 1. α is a constant ~0.5-1 [34]. This idea was borrowed from block copolymer field because indeed telechelic system can be considered as a tri-block copolymer. For this specific functionality, an unusual behaviour is evident when comparing the terminal and cluster relaxation times (Fig. 5): The cluster relaxation times exhibit a stronger temperature dependence than the terminal relaxation times, and both times might converge at lower temperatures. This behaviour corresponds to a negative B term in the expression for the effective interaction parameter (Fig. 9):

$$\chi = A + B/T \quad (8)$$

This behaviour is known for some block copolymers, especially for systems with hydrogen bonding [35-38]. It usually leads to a lower critical solution temperature (LCST). Estimates of χ using the Hansen solubility parameter approach [39] (see the Appendix) provides a value comparable to the experiment (Fig. 9), although this comparison does not have much value because the temperature dependence of χ – parameter is opposite to that expected in classical theory.

We emphasize that the SAXS measurements did not reveal any significant changes in morphology of the systems even down to 193K (Fig. 1b). Based on this result we suggest that though the two phases may be more miscible at lower temperatures (as would be implied with an LCST), the clusters might be locked in place at these temperatures because of their glassy state.

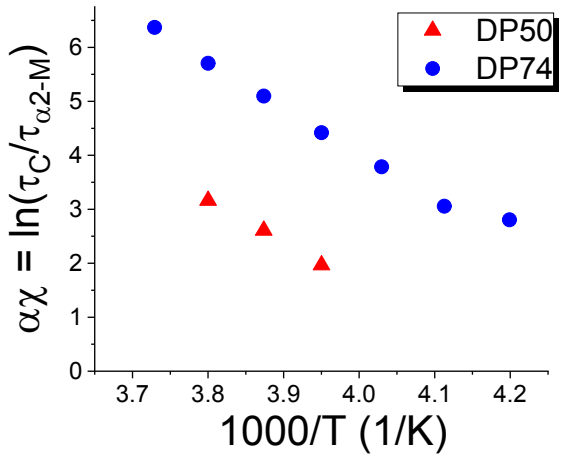

Fig 9. Temperature dependence of the Flory-Huggins interaction parameter estimated using eq. 7.

V. Conclusions

We presented a detailed analysis of dynamics in associating telechelic polymers with multiple hydrogen bonding stickers. Segmental relaxation of the polymers slows down with an increase of concentration of stickers leading to a nearly linear increase in T_g with the mole fraction of stickers. The latter agrees well with the recent theoretical predictions [25]. Both dielectric and rheological data revealed the existence of an intermediate relaxation process assigned to the binary stickers' dissociation and rearrangement processes. The energy barrier for the stickers dissociation appears relatively high, ~23 kJ/mol, as expected for multiple hydrogen bonds. This high energy barrier explains why the bond rearrangement and bond dissociation processes for the binary interactions have similar time scales.

The most interesting result is that the majority of these stickers form micro-phase separated clusters, as evidenced by SAXS data and the existence of the second T_g. We analysed the dynamics and terminal relaxation of these systems using the idea proposed in earlier studies [19, 20], which suggests that terminal relaxation is defined by the process of pulling a sticker from a cluster. This process is controlled by the structural relaxation time in the clusters with an additional energy barrier defined by the miscibility of the sticker with the polymer backbone, i.e. by the Flory-Huggins interaction parameter [30-33]. This mechanism enables control of terminal relaxation and viscoelastic properties of materials essentially independent of the polymer segmental relaxation. Detailed analysis of the dielectric and rheological data in the studied systems revealed a surprising result: the χ-parameter decreases upon cooling, suggesting potential LCST behaviour, where the stickers and polymer chain become more miscible with decreasing temperature. This behaviour is known for some block copolymers, especially those with hydrogen bonds [37, 38, 40]. We speculate that glass transition prevents the dissolution of clusters in the polymer matrix at lower temperatures preventing in this way observation of the expected LCST. This leads to a regime of rheological behaviour in which terminal flow is defined largely by structural relaxation in the clusters at lower temperatures, whereas it is delayed substantially beyond this time at higher temperatures when the stickers become less miscible in the polymer matrix. The presented results shed more light on the interplay between functional group cluster and backbone chain, allowing for more intelligent and precise design of functional materials with required viscoelastic properties.

VI. Appendix: Estimates of the Flory-Huggins interaction parameter using Hansen Solubility Parameter (HSP)

The χ-parameter can be roughly estimated using Hansen Solubility parameter (HSP) approach [39]. In this case,

$$\chi = \frac{(\delta_{end} - \delta_{PDMS})^2 V_{end}}{RT} \quad \text{(S1)}$$

Here δ_{end} and δ_{PDMS} are HSPs for the end group and PDMS backbone, respectively, and V_{end} is the volume of the end group. δ_{PDMS} is ~7.3 $cal^{1/2}cm^{-3/2}$ [41]. δ_{end} is estimated using HSP[34] that divides the solubility parameter into 3 partial components, δ_d - the dispersion part, δ_p - the polarity part and δ_{hb} - the hydrogen-bonding part. The total solubility parameter is calculated as

$$\delta_t = \sqrt{(\delta_d^2 + \delta_p^2 + \delta_{hb}^2)} \quad \text{(S2)}$$

Each partial parameter can be estimated through the group contribution method:

$$\delta_d = \left(\sum_i N_i C_i + \sum_j M_j D_j + 959.11\right)^{0.4126} (MPa)^{\frac{1}{2}}$$

(S3)

$$\delta_p = \left(\sum_i N_i C_i + \sum_j M_j D_j + 7.6134\right) (MPa)^{\frac{1}{2}} \quad \text{(S4)}$$

$$\delta_{hb} = \left(\sum_i N_i C_i + \sum_j M_j D_j + 7.7003\right) (MPa)^{\frac{1}{2}} \quad \text{(S5)}$$

where C_i is the contribution of the first-order groups of type i that appears N_i times in the compound and D_j is the contribution of the second-order groups of type j that appears M_j times in the compound.

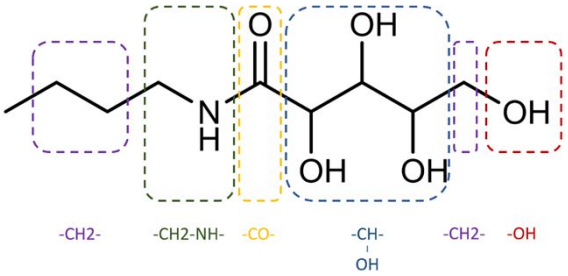

Fig A1. Chemical structure of chain ends dividing into 5 parts.

According to the multi-OH chain end structure, it possesses 4 different first-order groups (Fig. A1)[42]. By using the equations (eq. S6 – eq. S8), 3 partial parameters are calculated as shown below.

$$\delta_d = \left(3\delta_{d,CH2} + 3\delta_{d,CHOH} + \delta_{d,CO} + \delta_{d,OH} + \delta_{d,CH2NH} + 959.11\right)^{0.4126} = 16.95(MPa)^{\frac{1}{2}} \quad \text{(S6)}$$

$$\delta_p = \left(3\delta_{p,CH2} + 3\delta_{p,CHOH} + \delta_{p,CO} + \delta_{p,OH} + \delta_{p,CH2NH} + 7.6134\right) = 9.4703\ (MPa)^{\frac{1}{2}} \quad \text{(S7)}$$

$$\delta_{hb} = \left(3\delta_{hb,CH2} + 3\delta_{hb,CHOH} + \delta_{hb,CO} + \delta_{hb,OH} + \delta_{hb,CH2NH} + 7.7003\right) = 16.2708\ (MPa)^{\frac{1}{2}} \quad \text{(S8)}$$

Thus, $\delta_{end} = 25.33\ (MPa)^{\frac{1}{2}} = 12.38\ cal^{\frac{1}{2}}cm^{-\frac{3}{2}}$.

With V_{end} ~190 cm^3/mol, we estimate χ ~ 8.8 at T=270K. With the usual parameter α ~ 0.5 [32, 41, 43], $\alpha\chi$ will be in the range comparable to the experimental data in the Figure 9. However, the temperature dependence of the Flory-Huggins parameter (Fig. 9) is opposite to the expected in classical theory (eq. S1), leading to the LCST behaviour. The latter behaviour is known for many hydrogen bonding systems [35-38].

Authors Contributions

P.C., S.G. and S.S. performed all the measurements and data analysis, B.L. synthesized the polymers, A.P.S. developed the concept and led the research.

Conflicts of interest

There are no conflicts to declare.

Acknowledgments

This work was supported by the NSF Polymer program (**DMR-1904657**). X-ray measurements were made possible by the Major Research Instrumentation program of the National Science Foundation under Award No. **DMR-1827474**.

Notes and References

(1) Qin, B.; Zhang, S.; Sun, P.; Tang, B.; Yin, Z.; Cao, X.; Chen, Q.; Xu, J.-F.; Zhang, X. Tough and Multi-Recyclable Cross-Linked Supramolecular Polyureas via Incorporating Noncovalent Bonds into Main-Chains. *Advanced Materials* **2020**, *32* (36), 2000096. DOI: https://doi.org/10.1002/adma.202000096 (acccessed 2023/09/13).
(2) Cordier, P.; Tournilhac, F.; Soulié-Ziakovic, C.; Leibler, L. Self-healing and thermoreversible rubber from supramolecular assembly. *Nature* **2008**, *451* (7181), 977-980. DOI: 10.1038/nature06669.
(3) Li, C.-H.; Wang, C.; Keplinger, C.; Zuo, J.-L.; Jin, L.; Sun, Y.; Zheng, P.; Cao, Y.; Lissel, F.; Linder, C.; et al. A highly stretchable autonomous self-healing elastomer. *Nature Chemistry* **2016**, *8* (6), 618-624. DOI: 10.1038/nchem.2492.
(4) Cao, P.-F.; Li, B.; Hong, T.; Townsend, J.; Qiang, Z.; Xing, K.; Vogiatzis, K. D.; Wang, Y.; Mays, J. W.; Sokolov, A. P.; et al. Superstretchable, Self-Healing Polymeric Elastomers with Tunable Properties. *Advanced Functional Materials* **2018**, *28* (22), 1800741. DOI: https://doi.org/10.1002/adfm.201800741 (acccessed 2023/09/13).
(5) Peng, W.; Zhang, G.; Zhao, Q.; Xie, T. Autonomous Off-Equilibrium Morphing Pathways of a Supramolecular Shape-

Memory Polymer. *Advanced Materials* **2021**, *33* (34), 2102473. DOI: https://doi.org/10.1002/adma.202102473 (acccessed 2023/09/13).
(6) Cooper, C. B.; Nikzad, S.; Yan, H.; Ochiai, Y.; Lai, J.-C.; Yu, Z.; Chen, G.; Kang, J.; Bao, Z. High Energy Density Shape Memory Polymers Using Strain-Induced Supramolecular Nanostructures. *ACS Central Science* **2021**, *7* (10), 1657-1667. DOI: 10.1021/acscentsci.1c00829.
(7) Li, B.; Cao, P.-F.; Saito, T.; Sokolov, A. P. Intrinsically Self-Healing Polymers: From Mechanistic Insight to Current Challenges. *Chemical Reviews* **2023**, *123* (2), 701-735. DOI: 10.1021/acs.chemrev.2c00575.
(8) Samanta, S.; Kim, S.; Saito, T.; Sokolov, A. P. Polymers with Dynamic Bonds: Adaptive Functional Materials for a Sustainable Future. *J Phys Chem B* **2021**, *125* (33), 9389-9401. DOI: 10.1021/acs.jpcb.1c03511 From NLM.
(9) Ge, S.; Carden, G. P.; Samanta, S.; Li, B.; Popov, I.; Cao, P.-F.; Sokolov, A. P. Associating Polymers in the Strong Interaction Regime: Validation of the Bond Lifetime Renormalization Model. *Macromolecules* **2023**, *56* (6), 2397-2405. DOI: 10.1021/acs.macromol.2c02446.
(10) Yepremyan, A.; Osamudiamen, A.; Brook, M. A.; Feinle, A. Dynamically tuning transient silicone polymer networks with hydrogen bonding. *Chemical Communications* **2020**, *56* (88), 13555-13558, 10.1039/D0CC05478J. DOI: 10.1039/D0CC05478J.
(11) Porath, L. E.; Evans, C. M. Importance of Broad Temperature Windows and Multiple Rheological Approaches for Probing Viscoelasticity and Entropic Elasticity in Vitrimers. *Macromolecules* **2021**, *54* (10), 4782-4791. DOI: 10.1021/acs.macromol.0c02800.
(12) Chao, A.; Negulescu, I.; Zhang, D. Dynamic Covalent Polymer Networks Based on Degenerative Imine Bond Exchange: Tuning the Malleability and Self-Healing Properties by Solvent. *Macromolecules* **2016**, *49* (17), 6277-6284. DOI: 10.1021/acs.macromol.6b01443.
(13) Tress, M.; Ge, S.; Xing, K.; Cao, P.-F.; Saito, T.; Genix, A.-C.; Sokolov, A. P. Turning Rubber into a Glass: Mechanical Reinforcement by Microphase Separation. *ACS Macro Letters* **2021**, *10* (2), 197-202. DOI: 10.1021/acsmacrolett.0c00778.
(14) Ge, S.; Samanta, S.; Tress, M.; Li, B.; Xing, K.; Dieudonné-George, P.; Genix, A.-C.; Cao, P.-F.; Dadmun, M.; Sokolov, A. P. Critical Role of the Interfacial Layer in Associating Polymers with Microphase Separation. *Macromolecules* **2021**, *54* (9), 4246-4256. DOI: 10.1021/acs.macromol.1c00275.
(15) Eisenberg, A.; Hird, B.; Moore, R. B. A new multiplet-cluster model for the morphology of random ionomers. *Macromolecules* **1990**, *23* (18), 4098-4107. DOI: 10.1021/ma00220a012.
(16) Ricarte, R. G.; Tournilhac, F.; Leibler, L. Phase Separation and Self-Assembly in Vitrimers: Hierarchical Morphology of Molten and Semicrystalline Polyethylene/Dioxaborolane Maleimide Systems. *Macromolecules* **2019**, *52* (2), 432-443. DOI: 10.1021/acs.macromol.8b02144.
(17) Lessard, J. J.; Scheutz, G. M.; Sung, S. H.; Lantz, K. A.; Epps, T. H., III; Sumerlin, B. S. Block Copolymer Vitrimers. *Journal of the American Chemical Society* **2020**, *142* (1), 283-289. DOI: 10.1021/jacs.9b10360.
(18) Oba, Y.; Kimura, T.; Hayashi, M.; Yamamoto, K. Correlation between Self-Assembled Nanostructures and Bond Exchange Properties for Polyacrylate-Based Vitrimer-like Materials with a Trans-N-Alkylation Bond Exchange Mechanism. *Macromolecules* **2022**, *55* (5), 1771-1782. DOI: 10.1021/acs.macromol.1c02406.
(19) Ge, S.; Samanta, S.; Li, B.; Carden, G. P.; Cao, P.-F.; Sokolov, A. P. Unravelling the Mechanism of Viscoelasticity in Polymers with Phase-Separated Dynamic Bonds. *ACS Nano* **2022**, *16* (3), 4746-4755. DOI: 10.1021/acsnano.2c00046.
(20) Carden, P.; Ge, S.; Zhao, S.; Li, B.; Samanta, S.; Sokolov, A. P. Influence of Molecular Architecture on the Viscoelastic Properties of Polymers with Phase-Separated Dynamic Bonds. *Macromolecules* **2023**, *56* (13), 5173-5180. DOI: 10.1021/acs.macromol.3c00034.
(21) Mitchell, G. R.; Rosi-Schwartz, B.; Ward, D. J.; Warner, M.; Keller, A.; Warner, M.; Windle, A. H. Local order in polymer glasses and melts. *Philosophical Transactions of the Royal Society of London. Series A: Physical and Engineering Sciences* **1994**, *348* (1686), 97-115. DOI: doi:10.1098/rsta.1994.0083.
(22) Wu, S. Phase structure and adhesion in polymer blends: A criterion for rubber toughening. *Polymer* **1985**, *26* (12), 1855-1863. DOI: https://doi.org/10.1016/0032-3861(85)90015-1.
(23) F, K.; A, S. *Broadband Dielectric Spectroscopy;*; Springer-Verlag, 2003.
(24) Richert, R.; Wagner, H. The dielectric modulus: relaxation versus retardation. *Solid State Ionics* **1998**, *105* (1), 167-173. DOI: https://doi.org/10.1016/S0167-2738(97)00461-X.
(25) Ghosh, A.; Samanta, S.; Ge, S.; Sokolov, A. P.; Schweizer, K. S. Influence of Attractive Functional Groups on the Segmental Dynamics and Glass Transition in Associating Polymers. *Macromolecules* **2022**, *55* (6), 2345-2357. DOI: 10.1021/acs.macromol.2c00080.
(26) Ge, S.; Tress, M.; Xing, K.; Cao, P.-F.; Saito, T.; Sokolov, A. P. Viscoelasticity in associating oligomers and polymers: experimental test of the bond lifetime renormalization model. *Soft Matter* **2020**, *16* (2), 390-401, 10.1039/C9SM01930H. DOI: 10.1039/C9SM01930H.
(27) Zhang, Z.; Huang, C.; Weiss, R. A.; Chen, Q. Association energy in strongly associative polymers. *Journal of Rheology* **2017**, *61* (6), 1199-1207. DOI: 10.1122/1.4997586 (acccessed 9/13/2023).
(28) Chen, Q.; Tudryn, G. J.; Colby, R. H. Ionomer dynamics and the sticky Rouse modela). *Journal of Rheology* **2013**, *57* (5), 1441-1462. DOI: 10.1122/1.4818868 (acccessed 9/13/2023).
(29) Stukalin, E. B.; Cai, L.-H.; Kumar, N. A.; Leibler, L.; Rubinstein, M. Self-Healing of Unentangled Polymer Networks with Reversible Bonds. *Macromolecules* **2013**, *46* (18), 7525-7541. DOI: 10.1021/ma401111n.
(30) Ma, Y.; Lodge, T. P. Chain Exchange Kinetics in Diblock Copolymer Micelles in Ionic Liquids: The Role of χ. *Macromolecules* **2016**, *49* (24), 9542-9552. DOI: 10.1021/acs.macromol.6b02212.
(31) Wang, E.; Lu, J.; Bates, F. S.; Lodge, T. P. Effect of Corona Block Length on the Structure and Chain Exchange Kinetics of Block Copolymer Micelles. *Macromolecules* **2018**, *51* (10), 3563-3571. DOI: 10.1021/acs.macromol.7b02732.
(32) Wang, E.; Zhu, J.; Zhao, D.; Xie, S.; Bates, F. S.; Lodge, T. P. Effect of Solvent Selectivity on Chain Exchange Kinetics in Block Copolymer Micelles. *Macromolecules* **2020**, *53* (1), 417-426. DOI: 10.1021/acs.macromol.9b01877.
(33) Lu, J.; Bates, F. S.; Lodge, T. P. Chain Exchange in Binary Copolymer Micelles at Equilibrium: Confirmation of the Independent Chain Hypothesis. *ACS Macro Letters* **2013**, *2* (5), 451-455. DOI: 10.1021/mz400167x.
(34) Hansen, C. M. *Hansen solubility parameters: a user's handbook*; CRC press, 2007.
(35) Han, X.; Zhang, X.; Zhu, H.; Yin, Q.; Liu, H.; Hu, Y. Effect of Composition of PDMAEMA-b-PAA Block Copolymers on Their pH- and Temperature-Responsive Behaviors. *Langmuir* **2013**, *29* (4), 1024-1034. DOI: 10.1021/la3036874.
(36) Bütün, V.; Liu, S.; Weaver, J. V. M.; Bories-Azeau, X.; Cai, Y.; Armes, S. P. A brief review of 'schizophrenic' block copolymers. *Reactive and Functional Polymers* **2006**, *66* (1), 157-165. DOI: https://doi.org/10.1016/j.reactfunctpolym.2005.07.021.

(37) Kawata, Y.; Kozuka, S.; Yusa, S.-i. Thermo-Responsive Behavior of Amphoteric Diblock Copolymers Bearing Sulfonate and Quaternary Amino Pendant Groups. *Langmuir* **2019**, *35* (5), 1458-1464. DOI: 10.1021/acs.langmuir.8b01684.
(38) Schilli, C. M.; Zhang, M.; Rizzardo, E.; Thang, S. H.; Chong, Y. K.; Edwards, K.; Karlsson, G.; Müller, A. H. E. A New Double-Responsive Block Copolymer Synthesized via RAFT Polymerization: Poly(N-isopropylacrylamide)-block-poly(acrylic acid). *Macromolecules* **2004**, *37* (21), 7861-7866. DOI: 10.1021/ma035838w.
(39) Chremos, A.; Nikoubashman, A.; Panagiotopoulos, A. Z. Flory-Huggins parameter χ, from binary mixtures of Lennard-Jones particles to block copolymer melts. *The Journal of Chemical Physics* **2014**, *140* (5). DOI: 10.1063/1.4863331 (acccessed 4/1/2024).
(40) Lin, M.; Li, Z.; Fu, X.; Sun, J. Stimuli-responsive polypeptoid block copolymers containing o-nitrobenzyl groups with extremely sharp transition. *Journal of Polymer Science* **2023**, *61* (5), 385-390. DOI: https://doi.org/10.1002/pol.20220562 (acccessed 2023/12/04).
(41) Lee, J. N.; Park, C.; Whitesides, G. M. Solvent Compatibility of Poly(dimethylsiloxane)-Based Microfluidic Devices. *Analytical Chemistry* **2003**, *75* (23), 6544-6554. DOI: 10.1021/ac0346712.
(42) Stefanis, E.; Panayiotou, C. A new expanded solubility parameter approach. *International journal of pharmaceutics* **2012**, *426* (1-2), 29-43.
(43) Choi, S.-H.; Lodge, T. P.; Bates, F. S. Mechanism of Molecular Exchange in Diblock Copolymer Micelles: Hypersensitivity to Core Chain Length. *Physical Review Letters* **2010**, *104* (4), 047802. DOI: 10.1103/PhysRevLett.104.047802.